Breakup dynamic polarization potential for ^{6}He+^{208}Pb at 27 MeV

R. S. Mackintosh*
Department of Physics and Astronomy, The Open University, Milton Keynes MK7 6AA, United Kingdom

N. Keeley
CEA/DSM/DAPNIA/SPhN Saclay, 91191 Gif-sur-Yvette, France
(Received 17 March 2004; published 30 August 2004)

We study the local dynamic polarization potential, DPP, component of the ^{6}He+^{208}Pb interaction generated by the coupling to breakup channels as calculated using the continuum-discretized coupled-channels (CDCC) method. The results are for ^{6}He at a laboratory energy of 27 MeV. The elastic channel *S*-matrix is inverted and the bare potential of the CDCC calculation is subtracted to yield the DPP. This has a very long attractive and absorptive tail, with the real component extending beyond 40 fm, generated by Coulomb breakup. Although the long tail of the DPP has a major effect on the elastic *S*-matrix, it is shallow enough to have a more modest effect on the root mean square (rms) radius (increased) and the volume integrals. To facilitate comparison with other theories, the potential tails are fitted to analytic forms.

DOI: 10.1103/PhysRevC.70.024604 PACS number(s): 24.10.−i, 25.10.+s, 25.60.−t, 24.50.+g

I. INTRODUCTION

A full understanding of the interaction between pairs of nuclei requires an understanding of the contribution of excitation and transfer processes which occur as nuclei interact. In a recent paper [1] we discussed the local, *l*-independent representation of the dynamic polarization potential (DPP) arising from breakup processes for the case of protons scattering from ^{6}He. Such local DPPs are appropriate for evaluating theoretical descriptions of elastic scattering in terms of folding models with dynamic polarization corrections. In this paper we present a local *l*-independent representation of the DPP generated by projectile breakup for the elastic scattering of 27 MeV ^{6}He from ^{208}Pb. This DPP is generated with essentially the same model applied [1] to $p+^{6}$He scattering, but it has very different properties.

The calculations are conceptually straightforward: The elastic channel *S*-matrix, generated by continuum-discretized coupled-channels (CDCC) calculations of breakup processes, is subjected to $S(l)\rightarrow V(r)$ inversion. The bare potential of the CDCC calculations is then subtracted from $V(r)$ to yield the DPP. The inversion is carried out using the *iterative-perturbative*, IP, method [2–4], reviewed in [5], which generally gives reliable potentials at relevant radii. ^{6}He+^{208}Pb elastic scattering presents a very different challenge to IP inversion to that presented by ^{6}He+p scattering, adding to our general understanding of inversion. IP inversion is implemented in the code IMAGO [6].

II. ELASTIC SCATTERING AND BREAKUP OF ^{6}HE

Of necessity, a highly simplified model of ^{6}He is adopted, but one that appears to provide a useful description of $p+^{6}$He scattering, see discussion in [1,7]. The model is essentially that of [1,7], but with the omission of the $L=3$ continuum and the use of finer momentum bins, $\Delta k = 0.1$ fm^{-1}. The model was also employed in calculations [8] of ^{6}He+^{208}Pb at 29.6 MeV and in calculations [9] of ^{6}He+^{209}Bi at somewhat lower incident energies, 19.0 and 22.5 MeV. These references present figures showing the effect of the coupling on the elastic scattering partial differential cross-section; the effect is similar in the present case, and not shown here. The fit is qualitative, but no parameters are adjusted and, as noted above, many reaction channels must be omitted. The CDCC calculations were performed using the code FRESCO [10]. All inter-channel couplings are included; the importance of this is demonstrated in [1].

Many other reactions beside the breakup contributions modify the elastic scattering of ^{6}He. A full calculation including them all, respecting nonorthogonality terms, exchange processes, finite range transfer, etc. is a formidable task, and it could not be an aim of this work to determine the complete DPP.

Figure 1 compares $S(l)$ from the bare potential with the CDCC $S(l)$. The coupling generates a very long absorptive tail on $|S(l)|$ and an even longer attractive tail on arg $S(l)$. Inversion will confirm that the behavior of $S(l)$ when coupling is switched on corresponds to a very shallow but very long-ranged attractive and absorptive potential. In Sec. V we make explicit the distinctive contribution of Coulomb excitation.

For $l\leqslant 18$, the coupling increases $|S(l)|$. This apparently nonintuitive behavior has precedents and is discussed below. The effect of breakup on $S(l)$ for high l dominates the change in total reaction cross section which more than doubles from 1764 to 3652 mb.

III. INVERSION OF THE ELASTIC SCATTERING *S*-MATRIX

The natural starting potential for the iterative inversion procedure is the bare potential of the CDCC calculation. We reconstituted the bare potential by inverting the $S(l)$ from a calculation with coupling switched off. This was then

*Electronic address: r.mackintosh@open.ac.uk

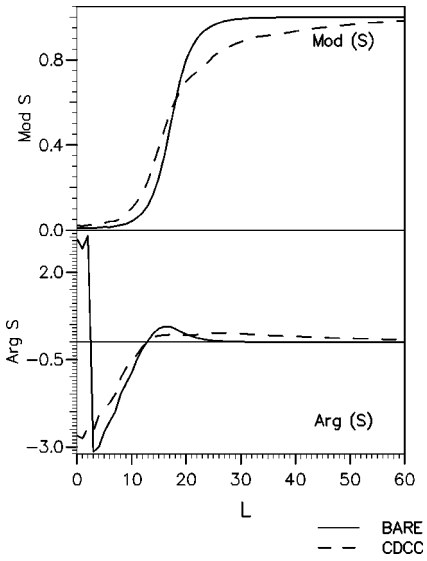

FIG. 1. For 27 MeV ^{6}He scattering from ^{208}Pb, $|S(l)|$ (above) and arg $S(l)$ (below) with the solid lines representing the uncoupled (bare potential) S-matrix and the dashed lines representing the full CDCC calculations.

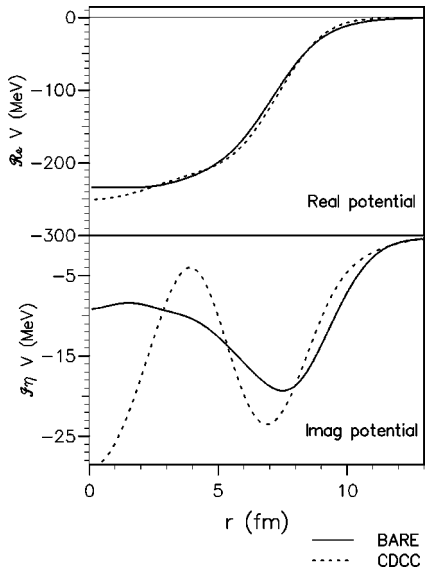

FIG. 2. Inverted potentials for 27 MeV ^{6}He scattering from ^{208}Pb for the radial range out to 13 fm. The solid line is the bare potential, the dashed line is for the CDCC calculation.

adopted as both the starting potential for subsequent inversions and as the bare potential to be subtracted from the potentials inverted from the CDCC elastic channel $S(l)$ to give the DPP. Since the DPP is the difference between two similar potentials, this procedure yields a DPP that is independent of any small differences between the way elastic scattering is calculated in the FRESCO and IMAGO codes.

When using the IP method, $S(l) \rightarrow V(r)$ inversion allows various different choices for the inversion basis [5]. Zero-order bessel functions were a suitable inversion basis for the bare $S(l)$, and did work for the full CDCC $S(l)$ in spite of the very large number of active partial waves in this case, far more than shown in Fig. 1, and the corresponding very long range of the DPP. Satisfactory inversion required a matching radius of 100 fm, and the inversion defined the potential out to this radius. Over 200 partial waves were included. The inversion was unable to fit certain slight irregularities in arg $S(l)$ for low l, and this prevented really low values of the "phase shift distance" [5] being achieved. The irregularities are possibly due to numerical instabilities in FRESCO arising from the low incident ^{6}He energy. Nevertheless, visually perfect fits to $S(l)$ were achieved over the rest of the range of l, except for very small oscillations for $l > 100$, where $1 - |S(l)|$ is very small in magnitude. Pursuing closer fits to $S(l)$ leads to oscillatory potentials and we present volume integrals and rms radii for three potentials which give successively closer fits to $S(l)$ at the cost of a small but increasing degree of oscillatory character. The solution that we have adopted as the CDCC potential is smoother than another with a slightly closer fit to $S(l)$; this is more easily seen when we present the DPPs below (Fig. 5).

In Fig. 2 we compare the adopted CDCC potential with the bare potential for $r \leqslant 13$ fm. The potential might be subject to some ambiguity for $r \leqslant 5$ fm, but it is for larger radii that the potential is of particular interest. In Fig. 3, we present the potentials between 13 and 40 fm. The imaginary and, even more, the real components have very long tails extending well beyond 40 fm. The imaginary tail is absorptive, as expected, and the real is attractive.

The properties of the potentials can be quantified in terms of the real and imaginary volume integrals per nucleon pair, J_{R} and J_{I}, and the corresponding rms radii, see Satchler [11]. The calculation of these moments requires care because of the nature of the long tails. The inverted potentials have very small amplitude oscillations at the largest radii which are of concern owing to the r^4 factor in the rms integrals. We, therefore, integrated out to cutoff radii of 70 fm for the real potential and 40 fm for the imaginary potential, which falls off more rapidly. These cut-off radii yield stable values of the

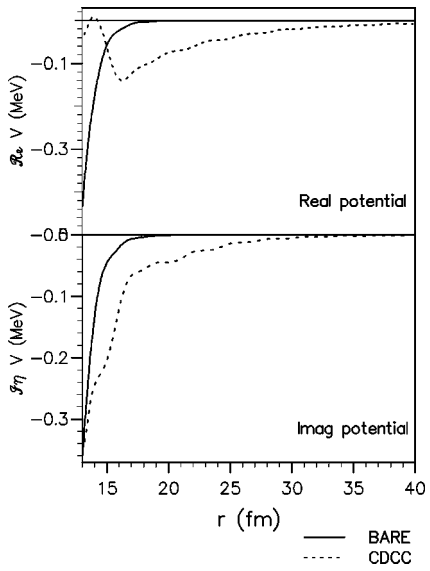

FIG. 3. As for Fig. 2, but covering the range from 13 to 40 fm.

TABLE I. Volume integral per nucleon pair J(MeV fm^3) and rms radii (fm) of the ^{6}He+^{208}Pb effective potentials representing the one-channel and CDCC calculations. The cut-off radii for the integrals are 70 fm (real parts) and 40 fm (imaginary parts), see text.

Case	J_R	$R_{rms,R}$	J_I	$R_{rms,I}$
Bare	320.41	6.588	57.20	8.323
CDCC, 4	312.68	8.588	54.72	9.132
CDCC, 5	312.51	8.609	54.69	9.135
CDCC, 6	312.20	8.541	52.81	9.112

respective quantities which are presented in Table I. The three CDCC solutions correspond to successively closer fits to $S(l)$, as mentioned above. The potential presented in Figs. 2 and 3 is "CDCC 5."

Despite the long but shallow attractive and absorptive tails of the CDCC potentials J_R, J_I are less than for the bare potential. In this sense, the coupling has had a slightly repulsive overall effect. Breakup increases the rms radius of the real component by 2 fm, but this does not give a measure of the extreme long range of the DPP. Although very shallow, the long tails lead to the substantial change in form shown by $S(l)$ in Fig. 1 as well as the doubling of the total reaction cross section.

IV. PROPERTIES OF DYNAMIC POLARIZATION POTENTIALS

Subtracting the bare potential from the CDCC potential yields the DPPs shown in Figs. 4 and 5. The real and imaginary components are comparable in magnitude, a general property of DPPs. Although very shallow beyond 13 fm, they have a major influence on scattering.

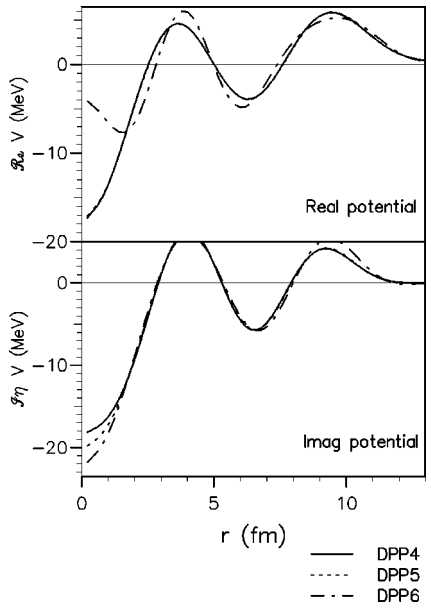

FIG. 4. For 27 MeV ^{6}He scattering from ^{208}Pb, the dynamic polarization potentials for the CDCC inverted potentials of Table I.

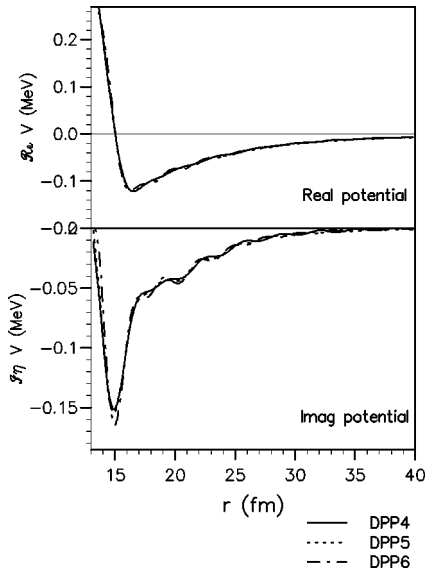

FIG. 5. As for Fig. 4, but covering the range from 13 to 40 fm.

The real component is attractive in the long tail, becoming repulsive as r falls below 13 fm and exhibiting oscillations further in. Such oscillations are not uncommon for a local l-independent representation of the DPP, which is l-dependent and nonlocal. The loosely bound ^{6}He must distort as it passes near or through the nucleus, and such distortion amounts to removal from the elastic channel. Insofar as it regains its shape as it leaves the nucleus, it returns to the elastic channel, a typical nonlocal effect [12]. The folding model implies that nonlocality for composite particles is short range [13], but this applies to exchange nonlocality arising from the knock-on exchange nonlocality for each nucleon.

Where the absorption is low, as in the far nuclear surface, the DPP is expected to be attractive, just as bound state energies are lowered when components are added. In the presence of strong absorption, the situation is different. The projectile propagates in a potential having strong radial gradients in both the real and imaginary parts. When the projectile is excited, momentum and angular momentum matching excitation spread its path; where it passes through a deeper real potential, it will also be more absorbed. An unabsorbed projectile, when it re-enters the elastic channel, will thus have acquired the phase corresponding to a shallower potential, registering as a repulsive DPP. The importance of the nature of the imaginary potential in determining the attractive or repulsive nature of the DPP has been discussed in Ref. [14] and references therein. Similar arguments show why, contrary to first expectations, coupling can, as here, lead to reduced absorption.

V. CONTRIBUTION OF COULOMB EXCITATION

We now report earlier calculations, carried out with a slightly nonoptimal bare potential, that bring out the role of Coulomb excitation. Figure 6 shows three sets of S-matrix elements: for all couplings switched off; with all nuclear

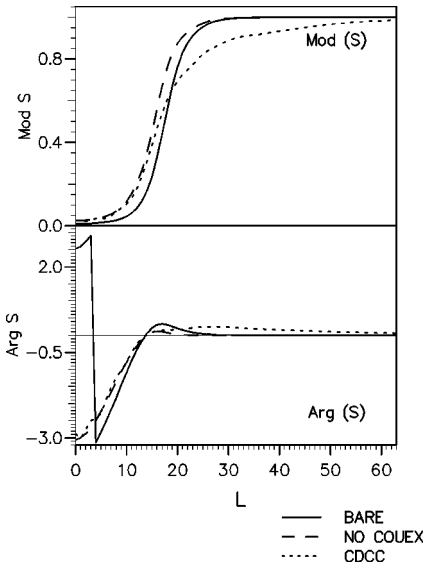

FIG. 6. For 27 MeV ^{6}He scattering from ^{208}Pb, $|S(l)|$ (above) and arg $S(l)$ (below) with the solid lines representing the uncoupled (bare potential) S-matrix, the dashed lines representing the cases with Coulomb coupling omitted, and the dotted lines representing the full CDCC calculations.

couplings included but with the Coulomb coupling omitted; and with all couplings included.

Pure nuclear coupling *increases* $|S(l)|$ for almost all the partial waves corresponding to nuclear overlap. The Coulomb coupling generates the long absorptive tail on $|S(l)|$ and even longer attractive tail on arg $S(l)$. For $l \leqslant 12$ the Coulomb excitation makes little difference to $S(l)$ so the decrease in absorption for low l is not related to Coulomb excitation.

The total reaction cross-section with no coupling is 1847 mb. With coupling but without Coulomb excitation, the total reaction cross-section *falls* to 1525 mb, corresponding to the increase in $|S(l)|$ over many values of l. Coulomb breakup increases the total reaction cross-section to almost double the original value: 3662 mb.

Displaced Gaussians provided a satisfactory inversion basis in this case. Although both the bare and inverted potentials are appreciably different from those presented in Sec. II, the DPPs are virtually identical, and the effect of the full coupling in Table II is very close to that in Table I. The DPPs

TABLE II. Volume integral per nucleon pair J(MeV fm^3) and rms radii (fm) of the ^{6}He+^{208}Pb effective potentials representing the one-channel and CDCC calculations. The cut-off radii for the integrals are 70 fm (real parts) and 40 fm (imaginary parts), see text.

Case	J_R	$R_{rms,R}$	J_I	$R_{rms,I}$
Bare	319.77	6.576	59.20	8.451
CDCC, No Couex	302.83	6.364	47.25	8.147
CDCC, 1	313.21	8.544	56.37	9.195
CDCC, 2	312.06	8.485	55.34	9.193
CDCC, 3	312.03	8.503	55.21	9.189

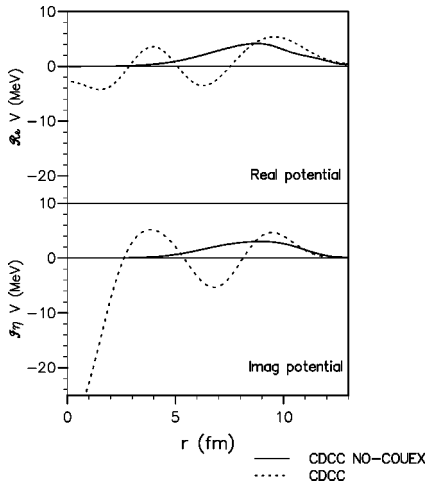

FIG. 7. For 27 MeV ^{6}He scattering from ^{208}Pb, the dynamic polarization potentials for the CDCC inverted potentials of Table II.

with and without Coulomb excitation are shown in Figs. 7 and 8. Coupling without Coulomb breakup leads to a reduction in the imaginary potential, in accord with the change in $|S(l)|$ in Fig. 6. The same is true for the full CDCC potential between 9 and 13 fm, but at smaller radii the potential exhibits a broad oscillation. Both J_R and J_I are reduced by coupling when the Coulomb term is omitted, as expected from Fig. 7.

VI. RELATION TO RECENT WORK

Kakuee *et al.* [15] have added a dipole Coulomb DPP, calculated using a semi-classical analytical expression, to a standard phenomenological potential for the present case. They show that it makes a substantial contribution to the elastic scattering angular distribution. Their formalism predicts that the imaginary potential becomes more important at higher scattering energies, something we can study in future work. They have also fitted the elastic scattering by varying phenomenological parameters, something that is difficult for

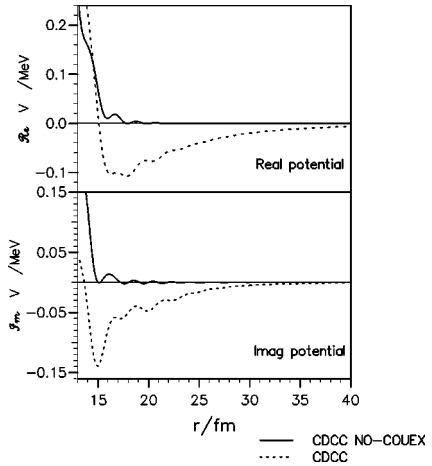

FIG. 8. As for Fig. 7, but covering the range from 13 to 40 fm.

us within the framework of a full CDCC calculation. They find an extremely large diffuseness parameter for the imaginary part. The present work suggests that the phenomenological potential might best be thought of as having a *component* of long range. We note their remark that there is an indication that "… there are reaction mechanisms that take flux out of the elastic channels at distances as large as 20 fm… an extraordinary result …" We agree.

Keeley *et al.* [9] contains further discussion of the breakup model that we have used, in particular establishing the reasonableness of the dipole strength, a critical factor in determining the magnitude of the long range DPPs. The ^{6}He+^{208}Pb elastic scattering data of Raabe [19] at 29.6 MeV are rather well described [8] by this breakup model, although the error bars are rather large. However, the description of the 27 MeV data of Kakuee *et al.* [15] is rather less good, suggesting that the Coulomb breakup component of the model is too large. This apparent discrepancy between the two energies could be accounted for by uncertainties in the position of the LAMP detector, discussed in detail in Kakuee *et al.* [15], changing the relative normalization of the forward and backward angle portions of the angular distribution at 27 MeV (there is an unfortunate gap in the crucial angular range due to the constraints of the experimental setup). Further data will be needed to clarify this issue.

A full comparison with the various semi-classical studies of Andrés *et al.* [16] and Canto *et al.* [17] as well as those of Kakuee [15] is clearly desirable. Since the dipole DPP is sensitive to details of the dipole strength function, a full comparison should involve the same nuclear model; a project to make such comparisons is clearly a priority for the future.

In the meantime, we have attempted to fit the tails of our potentials to powers or exponentials. Since there are no calculated errors on our potential, we express the goodness of fit with the statistical quantity R^2, as provided by Excel. The real potential CDCC-5 is quite well fitted between 17 and 70 fm by $V(r)=-1367.5r^{-3.2851}$, not exactly the inverse quartic predicted by Love *et al.* [18]. The statistical quantity R^2 was 0.986, indicating that the potential was well represented by this function, apart from oscillations in the tail. The real potential could not be fitted by an exponential. The imaginary part, on the other hand, could not be well-fitted by a power of r, but was fitted, between 17 and 40 fm, by $V(r)=-3.174\exp(-0.2173r)$ with $R^2=0.9796$, the departure of R^2 from unity being mostly due to oscillations about the exponential form. It would be interesting to include long range additive terms based on these forms in a phenomenological approach. There appear to be no semi-classical results relating to the inner regions of the interaction to which our potential can be compared.

VII. SUMMARY AND CONCLUSIONS

We have presented the local DPP generated by breakup of ^{6}He on ^{208}Pb at a laboratory energy of 27 MeV. The Coulomb contribution to breakup generates a DPP having a very shallow, very long ranged tail with a major effect on $S(l)$ over many partial waves and increasing the rms radius substantially. The surface attraction and absorption switch to repulsion and emissiveness as r falls below 13 fm. This emissiveness and repulsion in the DPP are not unique to this case, and are related to the strong absorptiveness of the bare potential. In principle, the bare potential should be adjusted to fit the cross-section of the full CDCC calculation but this was not done; reasonable changes to the bare potential will not alter the character of the DPP. There are many ways this work should be extended such as the inclusion of reaction channels and a more realistic model for ^{6}He.

The DPPs presented here show again that it is unphysical to represent dynamic polarization corrections to folding model potentials as a multiplicative correction factor.

[1] R. S. Mackintosh and K. Rusek, Phys. Rev. C **67**, 034607 (2003).
[2] R. S. Mackintosh and A. M. Kobos, Phys. Lett. **116B**, 95 (1982).
[3] A. A. Ioannides and R. S. Mackintosh, Phys. Lett. **169B**, 113 (1986).
[4] S. G. Cooper, V. I. Kukulin, R. S. Mackintosh, and V. N. Pomerantsev, Nucl. Phys. **A677**, 187 (2000).
[5] V. I. Kukulin and R. S. Mackintosh, J. Phys. G **30**, R1 (2004).
[6] S. G. Cooper, Open University report, unpublished.
[7] K. Rusek, K. W. Kemper, and R. Wolski, Phys. Rev. C **64**, 044602 (2001).
[8] K. Rusek, N. Keeley, K. W. Kemper, and R. Raabe, Phys. Rev. C **67**, 041604 (2003).
[9] N. Keeley, J. M. Cook, K. W. Kemper, B. T. Roeder, W. D. Weintraub, F. Maréchal, and K. Rusek, Phys. Rev. C **68**, 054601 (2003).
[10] I. J. Thompson, Comput. Phys. Rep. **7**, 167 (1988).
[11] G. R. Satchler, *Direct Nuclear Reactions* (Clarendon, Oxford, 1983).
[12] N. Austern, Phys. Rev. **137**, B752 (1965).
[13] D. F. Jackson and R. C. Johnson, Phys. Lett. **49B**, 249 (1974).
[14] R. S. Mackintosh and A. A. Ioannides, in the Int. Workshop Proceedings: '*Advanced methods in Evaluation of Nuclear Scattering data*, Lecture Notes in Physics Vol. 236 (Springer Verlag, Berlin, 1985), p. 283.
[15] O. R. Kakuee, J. Rahighi, A. M. Sánchez-Benítez, M. V. Andrés, S. Cherubini, T. Davinson, W. Galster, J. Gómez-Camacho, A. M. Laird, M. Lamehi-Rachti, I. Martel, A. C. Shotter, W. B. Smith, J. Vervier, and P. J. Woods, Nucl. Phys. **A728**, 339 (2003).
[16] M. V. Andrés, J. Gómez-Camacho, and M. A. Nagarajn, Nucl. Phys. **A579**, 273 (1994).
[17] Ł. F. Canto, R. Donangelo, P. Lotti, and M. S. Hussein, Nucl. Phys. **A589**, 117 (1995).
[18] W. G. Love, T. Terasawa, and G. R. Satchler, Nucl. Phys. **A291**, 183 (1977).
[19] R. Raabe, PhD thesis, Katholieke Universiteit Leuven, Leuven (2001).